Binding of Protoporphyrin IX and its H- and J-aggregates by Porphyrin-Binding Aptamer – Novel Candidates for Photosensitizer Delivery Systems and Method for Supporting Supramolecules

Karin Rogi and Akito Ishida*

Graduate School of Life and Environmental Sciences, Kyoto Prefectural University, Kyoto, Japan 606-8522

*Corresponding author: Graduate School of Life and Environmental Sciences, Kyoto Prefectural University, Kyoto, Japan *606-8522*. Email: a_ishida@kpu.ac.jp

Karin Rogi
Karin Rogi earned her master's degree in 2023 from Kyoto Prefectural University under the supervision of Professor Akito Ishida and bachelor's degree in 2021 from Kyoto Prefectural University. Her research focused on the photophysical and photochemical properties of photosensitizers in DNA aptamers.

Akito Ishida
Akito Ishida is a professor emeritus of Kyoto Prefectural University. His research mainly focused on the surface plasmon enhanced excitation of fluorescent molecules and surface plasmon enhanced polymerase chain reaction towards biomedical applications.

Abstract
The formation of protoporphyrin IX (PPIX) H- and J-aggregates and the interactions between porphyrin-binding aptamer (PBA), monomeric PPIX, and PPIX aggregates were comprehensively studied. The present study reveals for the first time that PBA can capture one or more PPIX molecules upon interaction with H- and J-aggregates forming the common novel complex, with the absorption maximum at 412 nm. This complex could not be prepared even by adding excess amount of monomeric PPIX to PBA. The titration experiments, and the denaturation and subsequent annealing of the resulting complex suggested the equilibrated interaction between PBA and H- or J-aggregates, and the affinity constants K_as were determined as 1.4×10^5 M^{-1} and 5.0×10^4 M^{-1}, respectively. From the standpoint of clinical applications, the aptamer sequence having affinity for cancer cells bound to the PBA sequence may be effective for drug delivery system of photodynamic therapy and diagnosis because the resulting complexes are sufficiently stable at body temperature to reach the target and are not too stable to release one or more PPIXs near cancer cells. From the standpoint of supramolecular chemistry, moreover, the present results may be useful for the immobilization of the porphyrin aggregates on the electrode or sensor surface using DNA aptamers for the practical applications.
Keywords: protoporphyrin IX, DNA aptamer, photodynamic sensitizer

Graphical Abstract

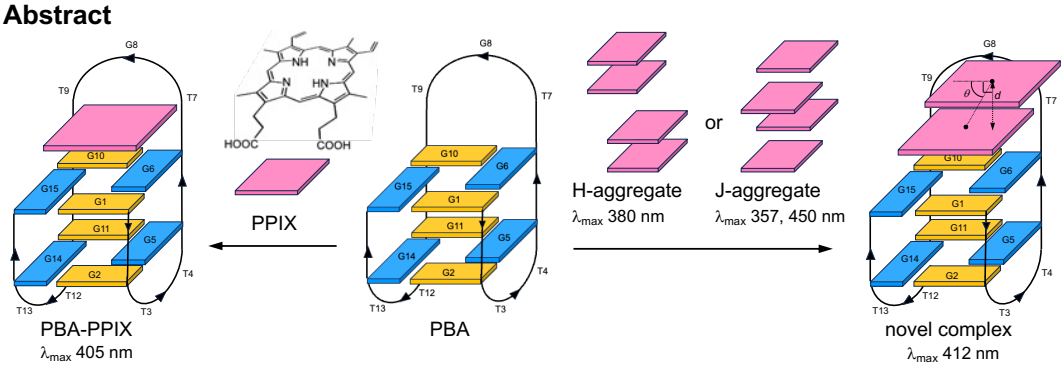

PBA can capture more than one PPIX molecules upon interaction with H- and J-aggregates forming the common novel complex, with the absorption maximum at 412 nm.

1. Introduction

DNA aptamers are artificially designed short DNA sequences that can bind to specific target molecules with high stabilization constants comparable to those of antibodies.[1–3] DNA aptamers have the following properties: Sequences for many types of target molecules can be designed based on computer simulations and artificial intelligence (AI).[4–6] Simple synthesis using a DNA synthesizer enables more rapid and inexpensive preparation of the desired aptamer compared with antibody preparation. The high chemical stability and biocompatibility of DNA aptamers, owing to the non-protein composition, make them suitable for clinical applications and long-term storage. Some DNA aptamers can bind to the surface of cancer cells even after binding to the target molecule.[7–9] Aside from the target-cell-recognition and binding properties of the aptamer sequence itself, the properties of the aptamer sequence can be further improved by modification of the 5'-NH_2 group introduced during DNA synthesis. The most typical example is folic acid, which has strong ability to recognize and bind to cancer cells that overexpress folate receptors on their surface.[10,11] Therefore, DNA aptamers are very suitable as drug carriers for targeting cancer cells.[12,13]

The application of DNA aptamers as photosensitizer (PS) carriers in photodynamic therapy (PDT) and diagnosis (PDD) has been widely studied. Porphyrins are particularly useful PSs as they effectively bind to DNA aptamers through intercalation into the guanine quadruplex (G4) of the DNA aptamers and electrostatic interactions. Although there are many detailed and precise studies on the interactions between aptamers and porphyrins, the target porphyrins used in almost all of these studies are limited to non-natural ionic porphyrins that possess high water solubility.[14–24] For example, the G-rich DNA aptamers AS1411 and 5,10,10-tetrakis(1-methylpyridinium-4-yl)porphyrin (TMPyP4) effectively afforded a G4/porphyrin complex via intercalation and external binding.[8] Because AS1411 recognizes the target cells of nucleolin,[7] the complex is expected to be used in practical PDT.

In contrast, protoporphyrin IX (PPIX), which is water-insoluble but inherently exists in living cells as a precursor of hemoglobin and can be effectively enriched by the administration of 5-aminolevulinic acid (ALA), is more suitable for PDT and PDD[25,26] than non-natural ionic porphyrins. Therefore, methods of enriching PPIX in cancer cells have been widely studied and improved.[27–30] PPIX is rapidly synthesized in cells after the administration of ALA, and the resulting PPIX is much more efficiently deposited in cancer cells than in normal cells, mainly due to the remarkable suppression of the activity of oxidative enzymes in cancer cells.[27] However, issues such as insufficient contrast in PDD and residual cancer cells after PDT resulting in the recurrence or metastasis are still persistent owing to the insufficient deposition of PPIX in the target cancer cells due to several factors such as the efflux of PPIX via exocytosis.[27]

From this perspective, the direct and effective delivery of PPIX to target cancer cells, in addition to the administration of ALA, may be preferable to a single dose of ALA. This methodology is promising for extinguishing clusters of cancer cells in lymph nodes by illumination using a fiber light, micro-LED, etc. Moreover, DNA aptamers bound to PPIX aggregates are expected to carry PPIX to cancer cells more effectively than those bound to the PPIX monomer. Based on this concept, we studied in this work the interaction between the porphyrin-binding aptamer (PBA) and PPIX itself (Fig. 1), as well as that between PBA and the supermolecules of PPIX, that is, the H- or J-aggregates, together with their efficient preparation.

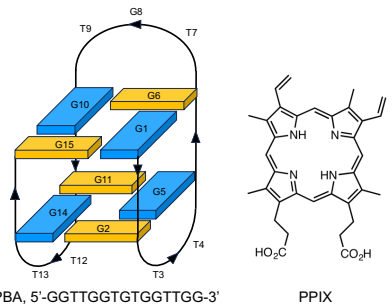

Fig. 1. The structures of antiparallel PBA and protoporphyrin IX (PPIX).

2. Experimental

2.1 Materials

Protoporphyrin IX (PPIX) (≥95%) was purchased from Sigma Aldrich and used without further purification. Tris(hydroxymethyl)aminomethane (Tris), dimethyl sulfoxide (DMSO), ethylenediaminetetraacetic acid disodium salt dihydrate (EDTA), NaCl, KCl, HCl, $NaHCO_3$, and polyethylene glycol mono-*p*-isooctylphenyl ether (Triton® X 100) were purchased from Nacalai Tesque, Inc. 6-Aza-2-thiothymine (ATT), diammonium hydrogen citrate (DAHC), and CH_3CN were purchased from FUJIFILM Wako Pure Chemical Co. A porphyrin-binding aptamer (PBA: GGT TGG TGT GGT TGG) was purchased from BEX Co. In all experiments, TNE buffer (10 mM Tris HCl, 200 mM NaCl, and 1 mM EDTA; pH 7) or Tris HCl buffer (10 mM Tris HCl, pH 7) was used to set the concentration of PPIX and its aggregates. In some cases, TNE and Tris-HCl buffers adjusted to pH 9 with $NaHCO_3$ were used. PBA was dissolved in TNE buffer (pH 7) or Tris-HCl buffer (pH 7) at a concentration of 1 mM and stored frozen. PPIX was dissolved to form a 1 mM stock solution in DMSO and stored. The stock solution was heated for 10 min before use. All experiments were performed at room temperature unless otherwise specified.

2.2 Measurement Apparatus

The absorption and fluorescence spectra of the small-scale samples were measured in a black-walled fluorescence microcell (light-path: 10 mm × 2 mm) or PCR tube using fiber optic spectrometers (Ocean Optics OP-FLAME-T, USB-2000, and QE-Pro). A D_2/W lamp (Ocean Optics) was used as the light source for the UV/vis absorption measurements. The cell temperature was controlled using a handmade precise temperature controller (Chino DB-1000Z). The solution temperature was measured using a Lake Shore 211 temperature monitor equipped with a ultra-micro Pt100 sensor dipped in the solution. The excitation source for the fluorescence measurement was a 405 nm laser diode (Thorlabs DL5146-101S) driven by a Thorlabs LDC-202C. The fluorescence spectra of the bulk-scale samples were obtained using a PerkinElmer LS55 fluorescence spectrometer. The spectral peak fitting was carried out using Fityk. The capillary electrophoresis measurements were carried out using an Agilent 7100. The matrix-assisted laser desorption-ionization time-of-flight mass spectra (MALDI-TOF-MS) were acquired using a MALDI TOFMS AXIMA® Performance instrument.

2.3 General Methods

The dilution and mixing procedures were crucial for this study because the aqueous solubility of PPIX is very poor. Reproduceable preparation of the samples, observations of the interactions, and the preparations of the weak complexes were only possible by the very careful dilution and/or mixing of the solutions. The very small amount of the solution made them more difficult. Rough and vigorous mixing will easily induce unexpected aggregation of the components resulting in the precipitation and/or reduced reproducibility. The specific detailed procedure was as follows. The tip end of the micropipette was carefully immersed into the buffer or PBA solution in a PCR tube or a microtube set into the cooling block, and then the solution of PPIX monomer or the aggregate was carefully and gently injected into the diluent followed by gentle repetitive pipetting for mixing without touching the inner surface of the tube by the tip end.

2.3.1 Thermal denaturation of PBA in the presence of potassium ions. A series of solutions containing 10 μM PBA and 0, 30, 40, and 100 mM KCl in Tris-HCl buffer (pH 7) was prepared and adjusted to pH 7 using Tris-HCl buffer (pH 9). The solutions were heated at 88°C for 10 min in PCR tubes using a thermal cycler, and then slowly cooled to room temperature. After annealing, 100 μL of the solution was carefully poured into the black-walled fluorescence microcell (light-path: 10 mm × 2 mm) without any bubbles. The cell was set into the temperature controller, and the absorption spectra were measured by scanning from 220 to 360 nm every 1°C while heating the solution from 25 to 72°C.

2.3.2 Thermal denaturation of PBA in the presence of sodium ions. A solution containing 10 μM PBA in TNE buffer (pH 7) was prepared. The solution was heated at 88°C for 10 min in PCR tubes using a thermal cycler, then slowly cooled to room temperature. After annealing, 100 μL of the solution was carefully poured into the black-walled fluorescence microcell (light-path: 10 mm × 2 mm) without any bubbles. The cell was set into the temperature controller, and the absorption spectra were measured by scanning from 220 to 360 nm every 1°C while heating the solution from 15 to 65 °C.

2.3.3 Mass spectrometry of PBA in the presence of potassium ions. A solution containing 100 μM PBA and 40 mM KCl in Tris HCl buffer (pH 7) was prepared and adjusted to pH 7 using Tris-HCl buffer (pH 9). The solution was heated at 88°C for 10 min, then slowly cooled to room temperature. MALDI-TOFMS data were acquired in linear-negative mode using 10 mg/mL ATT dissolved in CH_3CN:H_2O = 1:1 solution with 0.03 M DAHC as the matrix solution.

2.3.4 Preparation of PPIX monomer solution. PPIX (1 mM) was dissolved in DMSO as a stock solution. The stock solution was diluted with TNE buffer (pH 7) to prepare a series of 10 μM PPIX solutions containing 0.01, 0.02, 0.05, and 0.1% Triton® X 100.

2.3.5 Preparation of PPIX H- and J-aggregates. The detailed preparation methods for the PPIX H- and J-aggregates are described in the Results and Discussion section.

2.3.6 UV-vis absorption and fluorescence properties of PPIX monomer and H- and J-aggregates. The monomer or aggregate solution (100 μL) was carefully poured into a black-walled fluorescence microcell (light-path: 10 mm × 2 mm) without any bubbles. The UV-vis absorption spectra were measured using a 10 mm light-path, and the fluorescence spectra were measured by illumination with excitation light from the orthogonal direction with a light-path of 2 mm. Alternatively, the PCR tube filled with 20 μL of the solution was dipped into the specially prepared rectangular optical fiber coupler filled with water and the spectra were measured. The effective light-path was corrected using the absorbance of a standard solution. In these cases, the fluorescence measurements were performed using an orthogonal configuration.

2.3.7 Formation of PBA/PPIX complex. PPIX (12.5 μM) with 0.1% Triton® X 100 in TNE buffer (pH 7) was prepared from the stock solution of PPIX. The 1 mM PBA stock solution dissolved in TNE buffer (pH 7) was heated at 88 °C for 10 min, then slowly cooled to room temperature. The annealed PBA solution and the PPIX solution were mixed and diluted with TNE buffer (pH 7) to final concentrations of 200 μM PBA and 10 μM PPIX, respectively.

2.3.8 Thermal denaturation of PPIX monomer. PPIX (10 μM) and 0.02% Triton® X 100 were dissolved in Tris-HCl buffer (pH 7). The absorption spectra

spanning 350 to 800 nm were measured every 1 °C while heating the solution from 25 to 72°C.

2.3.9 Thermal denaturation of the PBA/PPIX complex in the presence of potassium ions. PBA (10 μM) and 40 mM KCl were dissolved in Tris-HCl buffer (pH 7). The pH of the solution was adjusted to 7 using Tris-HCl buffer (pH 9). The solution was heated at 88°C for 10 min and slowly cooled to room temperature. After annealing, 10 μM PPIX and 0.02% Triton® X 100 were dissolved in this solution. The absorption spectra spanning 350 to 800 nm were measured every 1°C while heating the solution from 25 to 50 °C.

2.3.10 Formation of PBA/PPIX H- or J-aggregate complexes in the presence of sodium ions and thermal denaturation. PBA stock solution (1 mM) dissolved in TNE buffer (pH 7) was heated at 88 °C for 10 min and then slowly cooled to room temperature. The H- and J-aggregate solutions were then prepared. The 1 mM PPIX stock solution dissolved in DMSO was diluted 10-fold with TNE buffer (pH 9) and then diluted with TNE buffer (pH 7) to obtain a final PPIX concentration of 12.5 μM. This solution is hereinafter called the H-aggregate solution. PPIX (12.5 μM) dissolved in TNE buffer (pH 7) was cooled on ice for 10 min. This solution is referred to as the J-aggregate solution. Finally, the PBA solution and the PPIX solution were mixed and diluted with TNE buffer (pH 7) so that the final concentrations were 200 μM PBA and 10 μM PPIX, respectively. The absorption spectra were measured in the range of 350–800 nm using a microcell with a light-path of 2 mm or a PCR tube. Thermal denaturation and subsequent annealing were carried out while measuring the absorption from 350 to 800 nm at increments of 1°C while heating the solution from 25 to 50°C, keeping 50°C for 1 h, and subsequent annealing from 50 to 25°C. The heating and cooling rate was 1°C /min.

3. Results and discussion

3.1 Stability of the G4 unit of PBA

Although the thermal properties of PBA have been reported,[31,32] we first studied the stability of the G4 unit by analyzing the UV spectral changes upon denaturation prior to studying the binding of PBA with the PPIX monomer and its aggregates in the present experimental conditions. It has been reported that the binding of K^+ to the central position of G4 effectively stabilizes the tertiary structure of an aptamer with a G4 unit.[33–37] Accordingly, PBA is thought to form a chair-like intramolecular antiparallel G4 unit in the presence of K^+.[36,38]

The UV absorption spectrum of the 10 μM PBA solution in Tris-HCl buffer (pH 7) showed an absorption maximum at 260 nm in the presence of 100 mM K^+ at 20°C (Fig. 2A). Upon heating the PBA solution to 72°C, the shape of the absorption spectrum changed with attenuation of the intensity of the peak at 295 nm, while maintaining an isosbestic point at 280 nm. The change in the absorbance at 295 nm was plotted against the temperature, yielding the denaturation curve of PBA (Fig. 2A, inset). The characteristic decrease in the intensity is attributable to denaturation, i.e., collapse of the G4 unit; the temperature at which half of the G4 collapsed was 49°C. The collapse temperature (T_m) was almost consistent with the reported values[31,32,39–41]. The T_m depended on the concentration of K^+. The titration experiment revealed that the minimum concentration of K^+ required for sufficient stabilization of G4 was 40 mM. A similar denaturation curve was observed in the TNE buffer containing 40 mM K^+.

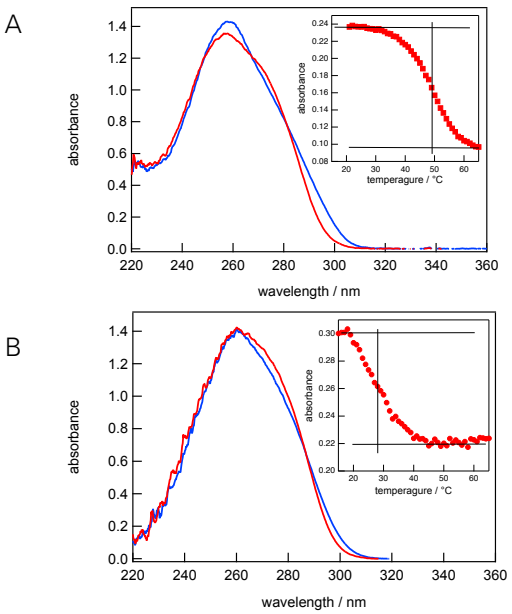

Fig. 2. The UV absorption spectra of the 10 μM PBA solution in pH 7 Tris-HCl buffer ([K^+]=100 mM) at 20°C (blue line) and 60°C (red line), A; in pH 7 TNE buffer ([Na^+]=200 mM)) at 20°C (blue line) and 40°C (red line), B; the insets show the denaturation curves of the absorbance at 295 nm.

In contrast with K^+, the stabilization effect of Na^+ was remarkably weak.[33,36,38,42] Even in the presence of 200 mM Na^+ (using TNE buffer), the T_m was 28 °C (Fig. 2B and inset), which is almost consistent with the reported value[39] and not much higher than that of cation-free PBA (26°C). However, the clear change in the absorption spectrum suggests that PBA also forms a characteristic chair-like tertiary structure, even in the presence of Na^+. Moreover, the low T_m suggests a looser and more flexible tertiary structure, which is preferable for binding large target molecules. In fact, interaction between the PBA and PPIX aggregates of PPIX was observed only in the presence of Na^+, as described hereinafter.

3.2 Interaction between PBA and monomeric PPIX

Although the interaction between PBA and monomeric PPIX is not the main focus of this study, we first studied this interaction because understanding the behavior of monomeric PPIX is

necessary for studying that of the aggregates as the reference. A 10 μM monomeric PPIX solution was prepared by high dilution of the stock DMSO solution of PPIX in the presence of 0.02% Triton® X 100 to slightly above the critical micellar concentration.[43] The sharp Soret band with a maximum at 405 nm in the UV-vis absorption spectrum indicated that the PPIX molecules were almost completely dispersed in the solution without considerable aggregation under these conditions (Fig. 3). Upon addition of 200 μM PBA (i.e., PBA:PPIX = 20:1) in the presence of 40 mM K^+ or 200 mM Na^+, both Soret bands showed slight hypochromic shifts (Fig. 3).

Under both ionic conditions, PBA was considered to form an antiparallel chair-like conformation. Accordingly, the resulting spectral changes could be attributed to the binding interaction between monomeric PPIX and the chair-like conformation of PBA. When the solutions were heated under both conditions, the Soret bands decreased with increasing temperature, forming a new broad absorption band at approximately 457 nm, with an isosbestic point at 431 nm. As discussed hereinafter, the new band was assigned to the J-aggregates of PPIX (Scheme 1). Because MALDI measurement of the 1:1 complex was not successful, we provide here the alternative evidence based on the photoelectrochemical measurement.[44]

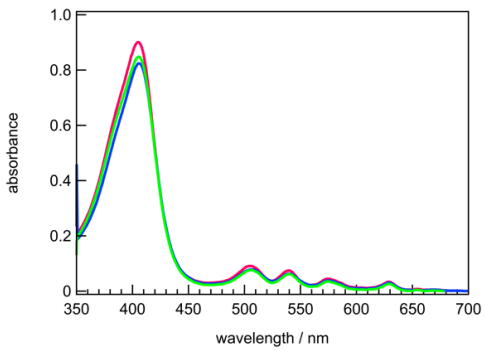

Fig. 3. UV-vis absorption spectra of 10 μM PPIX and 0.02% Triton® X-100 in the absence (in pH 7 Tris-HCl buffer, red line) and presence of 200 μM PBA (in pH 7 Tris-HCl buffer containing 40 mM K^+, green line; in pH 7 TNE buffer containing 200 mM Na^+, blue line).

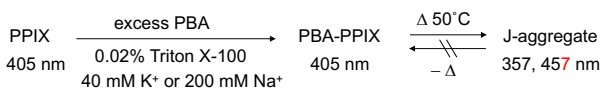

Scheme 1.

The thermal activation of the PBA framework induced distortion to release the PPIX monomers, which are expected to rapidly aggregate with each other to form the J-aggregate because the concentration of Triton® X 100 in the solution should be no longer too low to stabilize monomeric PPIX. In the presence of K^+ without PBA, the Soret band rapidly became less intense below 30°C, where the intensity was much lower than in the presence of PBA. These facts indicate that PBA, in the presence of K^+ or Na^+, effectively stabilizes PPIX to prevent aggregation, possibly by forming a 1:1 complex. We then focused on the differences in the effects of K^+ and Na^+ on the formation of the PBA-monomeric PPIX complex (PBA-PPIX). In the presence of K^+, the absorbance change of the Soret band upon heating was consistent with the denaturation curve of PBA, showing an identical inflection point at 49°C (Fig. 4). This suggests that the formation of PBA-PPIX did not significantly affect the stability of the rigid PBA framework in the presence of K^+. In contrast, in the presence of Na^+, the intensity of the Soret band decreased at a much higher temperature than in the denaturation curve of PBA, with an inflection point at 52°C (Fig. 4). As discussed above, the antiparallel framework of PBA containing two G4 units was effectively stabilized by the coordination of K^+ to the G4 units. On the other hand, the coordination of Na^+ was much weaker than that of K^+,[33–35,42] resulting in the much lower T_m of 28°C for the former.

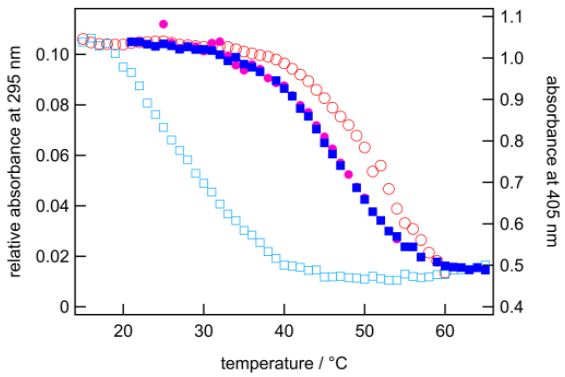

Fig. 4. The denaturation curves for the absorbances at the 295 nm of the 10 μM PBA in Tris-HCl buffer (pH 7) containing 200 mM Na^+ (aqua square □) and 40 mM K^+ (filled blue square ■), and for the 405 nm Soret band absorbances of the PPIX-PBA mixture in the presence of Na^+ (red circle ○) and K^+ (magenta filled circle ●).

The remarkable increase in the collapse temperature in the presence of Na^+ demonstrates that the PPIX molecule effectively stabilized the originally loose and flexible framework of PBA to form a more stable PPIX-PBA complex than that formed in the presence of K^+. The larger hypochromic shift observed in the presence of Na^+ than in the presence of K^+ also supports this assumption. Unfortunately, it was impossible to determine the association constant K_a between PBA and PPIX due to the very small intensity change of the Soret band. The fluorescence spectrum of monomeric PPIX showed maxima at 631 nm and 698 nm. Upon adding PBA in the presence of K^+ or Na^+, the intensities at 631 nm were lower than that of monomeric PPIX (Fig. 5). Although the fluorescence intensity is sensitively affected by several electronic and steric factors, this decrease in the fluorescence

intensity may be plausibly attributable to electronic interactions between PPIX and the G4 plane in the PPIX-PBA complex.

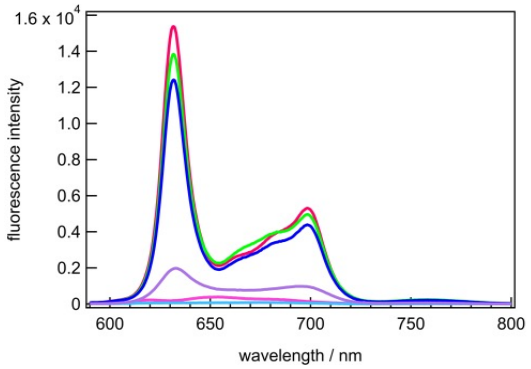

Fig. 5. Fluorescence spectra of 10 μM PPIX and 0.02% Triton® X-100 in the absence (in pH 7 Tris-HCl buffer, red line) and presence of 200 μM PBA in pH 7 Tris-HCl buffer containing 40 mM K^+, green line; in pH 7 TNE buffer containing 200 mM Na^+, blue line; the excitation wavelength was 405 nm: fluorescence spectra of the H- and J-aggregates and the 20:1 mixture of PBA and the H- aggregates are also shown as magenta, aqua, and purple lines, respectively; the excitation wavelengths were 380, 450, and 412 nm, respectively.

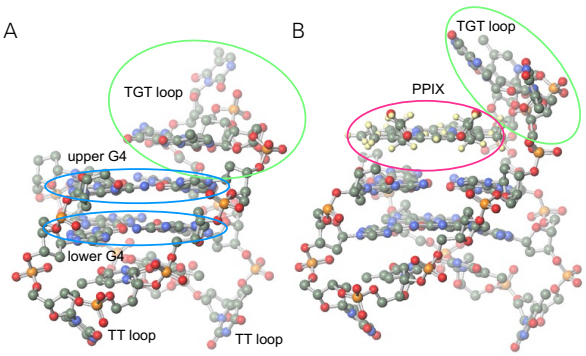

Fig. 6. The computer model of the thrombin aptamer (identical to PBA) based on the X-ray crystallographic data,[45] A; and the possible structure of PBA-PPIX, B.

It has been reported that cationic porphyrins, such as meso-tetrakis(*N*-methylpyridinium-4-yl) porphyrin, are bound to the outside of the quadruplexes by weak electrostatic interactions with the phosphate group of the sugar-phosphate backbone of PBA via electrostatic interaction, resulting in remarkable hypochromic and bathochromic shifts of the Soret band.[18] In contrast, PPIX has no positive charge. Therefore, binding with the phosphate groups via electrostatic interactions would be limited. The interaction between the electronic transitions of the PPIX and the G4 in PBA induced weak hypochromic and/or bathochromic shifts compared to those observed for the cationic porphyrins. However, PPIX effectively stabilized the chair-like conformation of PBA as described above, particularly in the presence of Na^+, indicating a tight binding interaction. Based on this presupposition and the experimental results, a PPIX unit may be drawn into the hydrophobic cavity between the upper G4 and the TGT loop, and then bound on the G4 mainly by hydrophobic interaction with lifting the TGT loop as shown in Fig. 6. The weak electronic interaction between the PPIX and the G4 may result in the weak spectral shifts. The access to the lower G4 plane seems to be more unfavorable because there are two short and rigid TT loops covering on the G4 plane.[45]

3.3 Selective preparation and photophysical properties of H- and J-aggregates

Several detailed and helpful studies on the formation, structure, and properties of H- and J-aggregates of PPIX in aqueous solutions are documented.[46–51] However, methods of preparing the aggregates must be established by ourselves prior to studying their interactions with PBA because the formation conditions were very restricted. It is well known that porphyrins easily form H- and J-aggregates owing to strong stacking interactions between the planar π-conjugated systems. The resulting exciton coupling in the H- and J-aggregates give rise to new characteristic absorption bands.[47,50,51]

In previous studies, H-aggregates of PPIX were obtained by high dilution of a DMSO solution of PPIX at pH > 9, whereas J-aggregates of PPIX were similarly obtained by high dilution at pH 7.[50] Therefore, herein, 10 μL of a 10 μM DMSO stock solution of PPIX was diluted with 2 mL of pH 9 TNE buffer to obtain H-aggregates. The absorption maximum of the resulting solution was 380 nm (Fig. 7, magenta line), which is consistent with the reported value for the H-aggregates.[50,51] In the present study, the dynamic light scattering (DLS) profile of the H-aggregates showed a single peak (96%) in the range of 4.5–40 nm, with a sharp maximum at 6.9 nm and a peak corresponding to an average particle size of 13.9 nm (Supplementary Fig. S1 panel A). Considering that the size of monomeric PPIX is approximately 2 nm, the component in the small range (4.5–6 nm) of the DLS profile may be attributed to the dimeric H-aggregate. However, the average particle size and the size of the peak tail were much larger than those of the dimers. Electrophoresis of the H-aggregates also revealed a single band with a weak tail. Thus, the as-prepared solution of the H-aggregates did not appear to contain only dimeric H-aggregates but also ordered H-aggregates consisting of different numbers of PPIX units. As suggested in previous studies, hydrogen bonding between the carboxyl groups of anti-type H-aggregates should contribute to the formation of highly ordered H-aggregates (Supplementary Scheme S1).[50] However, only the dimer peak of PPIX was observed by MALDI-TOF MS (Supplementary Fig. S2 Panel A), suggesting that the interactions between the H-aggregates forming the highly ordered structures were much weaker than those for the J-aggregates, as described below. Accordingly, the as-prepared

solution of the H-aggregates was used for further experiments.

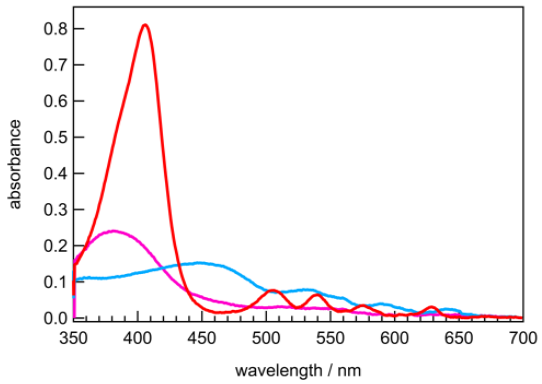

Fig. 7. UV-Vis absorption spectra of the monomeric 10 μM PPIX in TNE buffer (pH 7) in the presence of 1% Triton® X-100 (red line), the H-aggregates in TNE buffer (pH 9) (magenta line), and the J-aggregates in TNE buffer (pH 7) (aqua line).

J-aggregates of PPIX were obtained by highly diluting the stock solution in pH 7 TNE buffer. In contrast to the H-aggregates, the resulting solution showed two absorption bands with maxima at 357 and 457 nm (Fig. 7; aqua line), which were almost coincident with the reported values.[50,51] The most possible structures of the J-aggregates were proposed by Scolaro et al. as follows:[4] half-neutralization of the propionic acid side chains could induce very specific matching of the donor and acceptor hydrogen-bond sites, acting in an alternate fashion between adjacent porphyrins and dimers (Supplementary Scheme S1). As a result, highly ordered J-aggregates were easily grown. The growth of the highly-ordered J-aggregates was also supported by MALDI-TOF MS and DLS. Not only the dimer peak but also the peaks attributable to the highly-ordered aggregates was observed by the MALDI-TOF MS (Supplementary Fig. S2 Panel B). The DLS showed two peaks with a maximum at 11.6 nm (average size 23 nm, 31%) in the range of 11–40 nm as well as a peak with a maximum at 260 nm (average size 260 nm, 67%) in the range of 80–560 nm (Supplementary Fig. S1 panel B). The very large particle size was generally consistent with that observed in the scanning near-field optical microscope (SNOM) topography (173 nm).[50] This difference in the manner of hydrogen bonding may account for the DLS peaks corresponding to different particle sizes.

Because the as-prepared J-aggregate solution contained a sufficient fraction of small-sized aggregates, the as-prepared solution of J-aggregates was used for further experiments.

Band-shift analyses of the UV-visible absorption spectra of the H- and J-aggregates are very important for structural considerations of the aggregates. The interaction between the two transition dipoles splits the absorption band, which is known as excitonic coupling.[52,53] Excitonic coupling in the H- and J-aggregates of PPIX has previously been reported in detail.[50,51] The absorption maxima of the exciton bands, slip angles, and depolarization ratios are presented in Table 1. In the present study, we also observed characteristic band-shifts for the H- and J-aggregates (Fig. 7 and Table 1), similar to previous reports.[50,51]

Table 1. The photophysical properties of the PPXI, the H- and J-aggregates, and PPIX-PBA complexes

aggregate type		pH	absorption maximum / nm Soret band	Q-bands	emission / nm	slip angle θ
PPIX			405	506 539 574 630	631 698	
PBA-PPIX (K^+)			405	506 539 574 630	631 698	
PBA-PPIX (Na^+)			405	506 539 574 630	631 698	
H-aggregate	this work	9	380	509 579 619 655	653 683	90
H-aggregate	ref 50	12	382	510 545 578 626	624 684	90
H-aggregate	ref 51		384	512 582 639		
J-aggregate	this work	7	357 457	531 588 632 640	696	23
J-aggregate	ref 50	5	352 450			38 or 52
J-aggregate	ref 51		360 445	527 585 640		
PBA-H (H + PBA)			412	512 549 575 629	632 698	61
PBA-J (J + PBA)			412	513 546 578 633	632 698	61
H_4DPB	ref 56		379	511 540 580 632		

A possible arrangement for a H-aggregate is a head-to-tail arrangement of the two aromatic moieties, which can maximize the stacking interactions between the porphyrin cores and minimize the repulsion between the charged end groups.[50,51] It has been shown that π-π stacking interactions lead always to repulsion between the negatively charged clouds of the 22e aromatic porphyrin system, while σ-π interactions cause attraction between the rings.[54,55] As the result, a face-to-face arrangement with a lateral offset between the planes has been proposed as one of the lower energy dispositions for a porphyrin dimer.[54,55] However, the biphenylene-linked cofacial bisporphyrin (H_4DPB) showed an absorption maximum at 379 nm,[56] which was very consistent with that of the present H-aggregate (Table 1). The fact strongly suggested that the lateral offset should be minimal. Accordingly, we can assume the slip angle θ of the H-aggregate to be 90° and the orientation factor κ=1.

The square of the transition moment M^2 can be estimated by assuming the distance (d) of the PPIX rings of the H-aggregate within the stack as 3.6Å.[54,55] Based on the resulting M^2, we can estimate the slip angle θ of the J-aggregate as 23°. However, the very broad absorption bands may be attributed to the summation of the individual excitonic coupling modes, particularly in the J-aggregates with highly ordered complex geometries. Both of the H- and J-aggregates showed remarkably weaker fluorescence than that of the monomeric PPIX (Fig. 5). The substantial quenching indicates the strong electronic interactions of porphyrin units in the aggregates.

The four carboxyl groups of the H-aggregates formed at pH 9 should dissociate because the pK_a of PPIX is 4–5 and the resulting negative charges may repel each other. Scolaro et al. reported that the stability and structure of the aggregates strongly depend on the

ionic strength, because the added salt can screen the electrostatic repulsions between the four negatively charged dimers and stabilize the aggregated species through a series of specific interionic contacts.[50] Consequently, in the high-ionic-strength solution, the H-aggregates were converted to J-aggregates. However, in the present study, stable dimeric H-aggregates were successfully isolated for further studies, even in the TNE buffer containing 200 mM Na^+. Therefore, the interionic repulsion in the dimeric H-aggregates was expected to be effective in suppressing the conversion to J-aggregates.

3.4 Interaction between PBA and H- and J-aggregates of PPIX

The interaction between PBA and the H-aggregates of PPIX was studied. After mixing the PBA and H-aggregate solutions in a concentration ratio of 20:1 (PPIX equivalent, i.e., based on the preparation amount of PPIX), the UV-vis absorption spectra were continuously observed and recorded at 4 °C. The initially observed absorption band of the H-aggregate, with a maximum at 380 nm, rapidly disappeared soon after the mixing and gradually formed a new absorption band with a maximum at 412 nm, with an isosbestic point at 436 nm (Fig. 8A). The spectral change was almost completed after 3 h and the peak intensity was slightly enhanced for 24 h.

The species with 412 nm absorption gave rise to a fluorescence spectrum with maxima at 631 and 695 nm, similar to PBA-PPIX; the spectrum was rather broad, and the intensity was remarkably decreased to approximately 13% (Fig. 5). Therefore, the newly formed 412 nm-absorbing species was obviously different from the independently prepared PBA-PPIX, which showed the absorption maximum at 405 nm (Fig. 3) and much more intense fluorescence. In addition to that, the 412 nm-absorbing species was also obviously different from the parent H- and J-aggregates, both of which showed very weak fluorescence.

The denaturation experiment was carried out after completing formation of the 412 nm-absorbing species. The 412 nm band gradually decreased as the temperature increased and shifted to 403 nm, accompanied by a rise in the intensity of the shoulder around 380 nm (Fig. 8B). This change occurred below the collapse temperature of PBA in the presence of PPIX at 52°C. The change in the profile of the resulting 403 nm band during denaturation was obviously different from that of independently prepared PBA-PPIX and monomeric PPIX. Based on this fact and the spectral similarities, the resulting 403 nm band is not attributable to monomeric PPIX but to species that are structurally similar to PBA-PPIX, and the rise in the shoulder band around 380 nm is considered to be due to the recovered H-aggregates. When the solution was cooled after heating to 50°C, the intensity of the 403 and 380 nm bands simultaneously decreased and

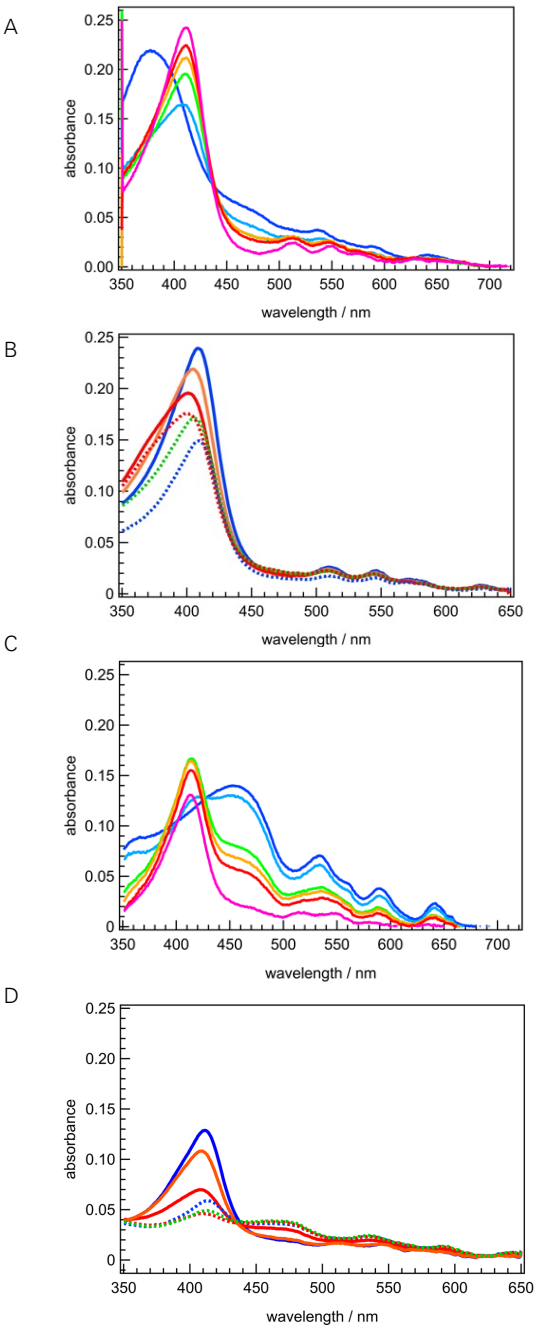

Fig. 8. The UV-Vis absorption spectral changes of the mixture of 100 μM PBA and the 5 μM H-aggregates (panel A) or J-aggregates (panel C) in TNE buffer containing 200 mM Na^+ at 4˚C measured before mixing (blue), after 10 s (aqua), 1 h (green), 2 h (orange), 3 h (red), and 24 h (magenta), respectively: the spectral change upon denaturation and subsequent cooling of the 412 nm-absorbing species prepared from the H-aggregates (panel B) and J-aggregates (panel D) measured at 25°C (solid blue line), 45°C (solid orange line), and 50°C (solid red line), respectively during heating; 50°C after 1 h (dotted red line), 40°C (dotted green line), 25°C (dotted blue line), respectively during subsequent cooling.

that of the 412 nm-absorbing species was partially recovered at 25°C (Fig. 8B). Therefore, the interaction between the PBA and H-aggregates was considered reversible. In the control experiment, independently prepared PBA-PPIX did not exhibit such a spectral shift during heating or subsequent cooling.

The titration experiment was carried out using the series of solutions containing the H-aggregates (5 μM in PPIX equivalent) and PBA (0, 2.5, 5, 10, 20, 40, 80, and 100 μM, respectively).

We assumed that PBA incorporated two PPIX molecules simultaneously, therefore the affinity constant K_a between PBA and H-aggregates can be estimated similarly to a simple 1:1 complex. Based on the absorbance change at 380 nm by using a double reciprocal plot (Supplementary Fig. S3), the affinity constant K_a was determined as 2.3×10^5 M^{-1}. This K_a was one order larger than that of the J-aggregates as discussed hereinafter. The difference is consistent with the remarkably more rapid disappearance of the H-aggregates after the mixing than the J-aggregates as shown in Fig. 8A and 8C.

The interaction between PBA and the J-aggregates of PPIX was also studied in a manner similar to that of the H-aggregates. After mixing the PBA and J-aggregate solutions at a concentration ratio of 20:1 (PPIX equivalent), the absorption band of the J-aggregate with a maximum at 457 nm decreased, accompanied by the appearance of a new band at 412 nm, with an isosbestic point at 428 nm (Fig. 8C). The spectral change was slower than that of the H-aggregate but was almost completed after 3 h, and the resulting 412 nm band approximately 20% decreased after 24 h. The maximum absorbance of the 412 nm band was 0.17, which is remarkably smaller than that of the H-aggregate, 0.24. At a concentration ratio of 1:1, J-aggregates remained after 3 h and the conversion was not complete. Therefore, the interaction between PBA and the J-aggregates was obviously less efficient than that between PBA and the H-aggregates. A denaturation experiment was also carried out for the J-aggregates. The 412 nm band gradually decreased as the temperature increased and shifted to 407 nm, accompanied by a rise in the intensity of the shoulder peak at approximately 470 nm (Fig. 8D). This change occurred below the collapse temperature of PBA in the presence of PPIX at 52°C. The change in the resulting 408 nm band during denaturation was very similar to that of the 403 nm band of the H-aggregates. Based on this fact and the similarities of the spectra to the literature data, the resulting 407 nm band is attributable to species having a structure similar to that of PBA-PPIX, and the simultaneously formed 470 nm band is attributed to recovered J-aggregates. When the solution was cooled after heating to 50°C, the 408 nm and 470 nm bands simultaneously decreased, and the 412 nm-absorbing species was partially recovered at 25°C.

The titration experiment was carried out using the series of solutions containing the J-aggregates (5 μM in PPIX equivalent) and PBA (0, 2.5, 5, 10, 20, 40, 70, and 100 μM, respectively). From the absorbance change at 457 nm (Supplementary Fig. S4), the affinity constant K_a between PBA and the J-aggregates was determined as 4.7×10^4 M^{-1}. Although the interaction between PBA and the J-aggregates is also considered reversible, the recovery was obviously less efficient than that of the H-aggregates because the 470 nm band still persisted after reaching the steady state (Fig. 8B). The fact may be consistent with the smaller K_a of the J-aggregates than that of the H-aggregates.

Notably, denaturation of the independently prepared PBA-PPIX simply released monomeric PPIX from the PBA framework irreversibly to form only the J-aggregates. Accordingly, the peak of the 412 nm-absorbing species does not merely arise from a spectral shift of PBA-PPIX itself induced by conformational change and/or the change in the electronic environment surrounding the PPIX unit in the 1:1 complex. The existence of the 412 nm-absorbing species was also confirmed by capillary electrophoresis of the mixture of the J-aggregates and PBA (Supplementary Fig. S5). We again emphasize that the 412 nm-absorbing species could not be formed by simple mixing of PBA and monomeric PPIX.

Based on the above results, we can assume that the H- and J-aggregates both interact with PBA to form a common 412 nm-absorbing species. Here, we discuss the structure and properties of the 412 nm-absorbing species. Notably, the formation of the 412 nm-absorbing species was only observed upon adding PBA prepared in the presence of 200 mM Na^+. In contrast, in the presence of 100 mM K^+, neither the H- nor J-aggregates changed after mixing with PBA. As discussed above, the chair-like tertiary structure of PBA in the presence of Na^+ is looser and more flexible, corresponding to a much lower T_m than that in the presence of K^+. Accordingly, the loose and flexible tertiary structure of PBA should be necessary for forming the 412 nm-absorbing species by interaction with the H- or J-aggregates.

The spectral changes upon denaturation and subsequent cooling indicate that the 412 nm-absorbing species dissociated into PBA-PPIX and the corresponding parent aggregates upon denaturation, which recombined with each other to recover the 412 nm-absorbing species upon cooling. Therefore, the interaction between the 412 nm-absorbing species, PBA-PPIX, and H- or J-aggregates was considered to be in equilibrium, as shown in Scheme 2. Moreover, the PBA-PPIXs derived from the H- and J-aggregates showed similar denaturation profiles, and the T_m values were higher than those of the independently prepared PBA-PPIXs. This demonstrates that the parent H- and J-aggregates stabilize PBA-PPIX formed upon denaturation in the solution, possibly by adhering to each other giving PBA-PPIX···H and PBA-PPIX···J,

respectively. This weak interaction may be due to the slight band shifts of the PBA-PPIX···H (403 nm) and PBA-PPIX···J (407 nm) from the independently prepared PBA-PPIX (405 nm).

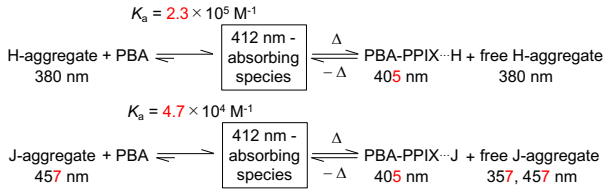

Scheme 2.

The discussion thus far leads to the assumption that the structure of the 412 nm-absorbing species comprises more than one PPIX unit, and is probably the dimer, which interacts with the G4 units of PBA. However, the stoichiometry of the complex is speculative, because the direct structural evidence could not be obtained by commonly used methods such as MALDI, NMR, etc. due to many technical restrictions. Therefore, we were forced to rule out other possibilities as follows.

The computer model of the chair-like structure from X-ray crystallography shown in Fig. 6 suggests that the TGT and TT loops, which play a significant role in the recognition of thrombin, may prevent the access of more than one PPIX molecule to the G4 planes, particularly in the presence of K^+ ions, resulting in a rigid framework of PBA.[45] On the other hand, the stability of the 1:1 complex was indicated by the electrochemical measurement[44] as described above. Accordingly, the access of the two PPIX units should require a certain degree of flexibility of the PBA flamework. This assumption is consistent with the observed formation of the 412 nm-absorbing species only in the presence of Na^+ ions. The weak stabilization effect of the G4 units by Na^+ allowed the conformational change of the TGT and/or TT loops so that more than one PPIX molecule from the H- or J-aggregates could access the G4 planes, probably the upper G4 plane by pulling up the rather flexible TGT loop similarly to the PBA-PPIX, mainly due to hydrophobic interaction as shown in Fig. 9. The access to the lower G4 plane seems to be more unfavorable because the TT loops covering on the lower G4 plane seem to be too short and rigid[45] to stabilize the PPIX units by steric and/or electronic effect.

Considering the high fragility, the spatial congestion on the G4 planes, sufficient stability of the 1:1 complex, and the equilibrium and reversible interaction of H- or J-aggregates with PBA, the formation of the 1:2 complex should be the most reasonable.

Consequently, the electronic conditions surrounding the PPIX units give a common absorption band at 412 nm, which is consistent with the exciton coupling band corresponding to the two most overlapping porphyrin rings. Assuming that the center-to-center distance of the PPIX rings and the transition moment are similar to that of the H- and J-aggregates as discussed the above, the slip angle θ of the 412 nm-absorbing species is calculated as 61°. The slip angle was remarkably different from that of the H- and J-aggregates, 90° and 23°, respectively. Therefore, the two porphyrin rings were forcibly slid with the specific slip angle, θ from the original configurations of the H- and J-aggregates with the support of G8 and T7 on the TGT loop of PBA, as shown in Fig 9. The resulting electronic interaction between the PPIX units was considered to be weaker than that of the parent aggregates, but stronger than that of PBA-PPIX, leading to the moderate fluorescence intensity as shown in Fig. 5. The average size of the H-aggregates was remarkably smaller than that of the J-aggregates as described above. The compact size of the H-aggregates may be preferable to the complexation with PBA giving the larger K_a than the J-aggregates.

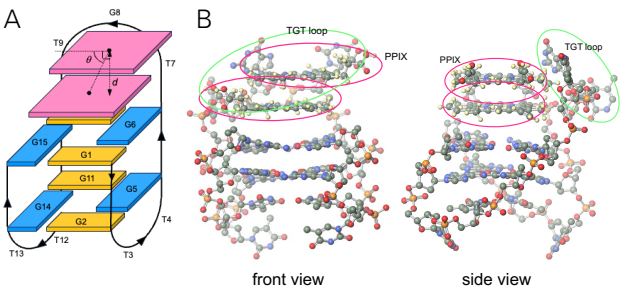

Fig. 9. The schematic diagram (A) and computer models (B) of proposed structure of the 412 nm-absorbing species. A PPIX plane is shown as a pink panel and pink circled in the schematic diagram and models, respectively.

The complete disappearance of the aggregates soon after mixing with an excess amount of PBA suggests the effective degradation of the aggregates and simultaneous incorporation of the PPIX units into the PBA framework. The resulting 412 nm-absorbing species was partially degraded during denaturation, releasing one of the incorporated PPIX molecules, which may be rapidly dragged into the parent aggregates and remain in the solution, causing partial recovery of the absorption bands of the aggregates. In contrast, another PPIX remained in the PBA framework as PBA-PPIX until completion of the collapse.

Although we repeatedly attempted to obtain direct and clear evidence of the molecular composition of the 412 nm-absorbing species, i.e. the ratio of PPIX and PBA, by MALDI-TOF-MS, we could not obtain clear results at present because of the high salt concentration and decomposition during the ionization. However, not only simple absorption spectroscopy, but also capillary electrophoresis of the mixtures of PBA and monomeric PPIX, PBA and the J-aggregates

gave apparently different absorption maxima at 405 nm and 412 nm, respectively (Supplementary Fig. S5). The fact and the denaturation properties indicate that both PBA-PPIX and the 412-nm absorbing species exist as stable supramolecular complexes at room temperature.

4. Conclusion

The formation of PPIX aggregates and the interactions between PBA, monomeric PPIX, and PPIX aggregates were comprehensively studied. Although important for biomedical and supramolecular research, this type of study has not been attempted because of the serious experimental difficulties caused by the very poor aqueous solubility of PPIX and the aggregates, and by the fragility of the complexes. The present study reveals for the first time that PBA can capture more than one PPIX molecules upon interaction with H- and J-aggregates. From the standpoint of clinical applications, the resulting complexes are sufficiently stable in a buffer solution at body temperature to reach the target cancer cells and are not too stable to release one or more PPIXs nearby the targets. Therefore, the aptamer sequence having affinity for cancer cells bound to the PBA sequence should be effective DDS for PPIX, in accordance with the aim of this study described in the Introduction.

Moreover, the present results may be extended to a novel supramolecular chemistry methodology. Although very interesting meta-stable three-dimensional molecular aggregates have been reported, many are unstable and impossible to isolate and immobilize on the electrode or sensor surface for practical applications. The soft covering of the aggregates by aptamers may provide an avenue for overcoming these difficulties. Thus, aptamer-based supramolecular chemistry may be a promising topic for next-generation supramolecular chemistry.

Acknowledgement

The authors are grateful to Mr. Taizo Hasegawa and Mr. Shinsuke Hashida of Otsuka Electronics Co. Ltd. for facilitating the capillary electrophoresis measurements.

Supplementary data

Supplementary material is available at *Bulletin of the Chemical Society of Japan.*

Funding

This work was partly supported Kyoto funding for Innovation in Health-related R&D Fields, Kyoto City Hall and Kyoto Lifetech Innovation Support Center (KLISC), Japan.

Conflict of interest statement. None declared.

References

1 Y. Zhang, B. S. Lai, M. Juhas, *Molecules*, **2019**, *24*, 941.
2 S. D Jayasena, *Clin. Chem*, **1999**, *45*, 1628.
3 L. Gold, N. Janjic, T. Jarvis, D. Schneider, J. J. Walker, S. K. Wilcox, D. Zichi, *Cold Spring Harb Perspect. Biol.,* **2012**, *4*, a003582.
4 Z. Chen, L. Hu, B. T. Zhang, A. Lu, Y. Wang, Y. Yu, G. Zhang, *Int. J. Mol. Sci.*, **2021**, *22*, 3605.
5 S. J. Lee, J. Cho, B. H. Lee, D. Hwang, J. W. Park, *Biomedicines*, **2023**, *11*, 356.
6 A. Di Gioacchino, J. Procyk, M. Molari, J. S. Schreck, Y. Zhou, Y. Liu, R. Monasson, S. Cocco, P. Šulc, *PLoS. Comput. Biol.*, **2022**, *18*, e1010561.
7 E. M. Reyes-Reyes, Y. Teng, P. J. Bates, *Cancer Res.,* **2010**, *70*, 8617.
8 Y. A. Shieh, S. J. Yang, M. F. Wei, M. J. Shieh, *ACS Nano* **2010**, *4*, 1433.
9 J. Carvalho, A. Paiva, Cabral Campello, Maria Paula, A. Paulo, J. L. Mergny, G. F. Salgado, J. A. Queiroz, C. Cruz, *Sci Rep* **2019**, 9, 7945.
10 Yehuda G. Assaraf, Christopher P. Leamon, Joseph A. Reddy, *Drug resistance updates* **2014**, *17*, 89.
11 Nikki Parker, Mary Jo Turk, Elaine Westrick, Jeffrey D. Lewis, Philip S. Low, Christopher P. Leamon, *Anal Biochem* **2005**, *338*, 284.
12 Z. Wei, Y. Zhou, R. Wang, J. Wang, Z. Chen, *Pharmaceutics* **2022**, *14*, 2561.
13 Partha Ray, Rebekah R. White, *Pharmaceuticals* **2010**, *3*, 1761.
14 Y. Li, C. R. Geyer, D. Sen, *Biochemistry* **1996**, *35*, 6911.
15 H. Yaku, T. Murashima, D. Miyoshi, N. Sugimoto, *Molecules* **2012**, *17*, 10586.
16 Y. A. Lee, S. Lee, T. S. Cho, C. Kim, S. W. Han, S. K. Kim, *Journal of Physical Chemistry B* **2002**, *106*, 11351.
17 W. Zhou, Y. Cheng, B. Song, J. Hao, W. Miao, G. Jia, C. Li, *Biochemistry* **2021**, *60*, 3707.
18 I. Haq, J. O. Trent, B. Z. Chowdhry, T. C. Jenkins, *J Am Chem Soc* **1999**, *121*, 1768.
19 G. Song, J. Ren, *Chemical Communications* **2010**, *46*, 7283.
20 N. V Anantha, M. Azam, R. D. Sheardy, *Biochemistry* **1998**, *37*, 2709.
21 M. del Toro, R. Gargallo, R. Eritja, J. Jaumot, *Anal Biochem* **2008**, *379*, 8.
22 D. Zhao, X. Dong, N. Jiang, D. Zhang, C. Liu, *Nucleic Acids Res.*, **2014**, *42*, 11612.
23 I. R. Krauss, A. Merlino, C. Giancola, A. Randazzo, L. Mazzarella, F. Sica, *Nucleic Acids Res.*, **2011**, *39*, 7858.
24 H. Y. Cho, Y.-A. Lee, Y. S. Oh, G. J. Lee, Y. J. Jang, S. K. Kim, *J. Biomol. Struct. Dyn.*, **2020**, *38*, 2686.
25 E. Yoshioka, V. S. Chelakkot, M. Licursi, S. G. Rutihinda, J. Som, L. Derwish, J. J. King, T. Pongnopparat, K. Mearow, M. Larijani, A. M. Dorward, K. Hirasawa, *Theranostics*, **2018**, *8*, 2134.
26 H. Fukuhara, K. Inoue, A. Kurabayashi, M. Furihata, T. Shuin, *BMC Urol.*, **2015**, *15*, 78.
27 Y. Kitajima, T. Ishii, T. Kohda, M. Ishizuka, K. Yamazaki, Y. Nishimura, T. Tanaka, S. Dan, M. Nakajima, *Sci. Rep.*, **2019**, *9*, 8666.
28 K. Omoto, R. Matsuda, Y. Nakai, Y. Tatsumi, T. Nakazawa, Y. Tanaka, Y. Shida, T. Murakami, F. Nishimura, I. Nakagawa, Y. Motoyama, M. Nakamura, K. Fujimoto, N. Hiroyuki, *Photodiagnosis Photodyn. Ther.*, **2019**, *25*, 309.
29 M. Kiening, N. Lange, *Int. J. Mol. Sci.*, **2022**, *23*, 7974.

30 V. S. Chelakkot, K. Liu, E. Yoshioka, S. Saha, D. Xu, M. Licursi, A. Dorward, K. Hirasawa, *Sci. Rep.*, **2020**, *10*, 22124.

31 O. Tatarinova, V. Tsvetkov, D. Basmanov, N. Barinov, I. Smirnov, E. Timofeev, D. Kaluzhny, A. Chuvilin, D. Klinov, A. Varizhuk, G. Pozmogova, *PLoS One*, **2014**, *9*, e89383.

32 Roman F. Macaya, Peter Schultze, Flint W. Smith, James A. Roe, Juli Feigon, *Proc. Natl. Acad. Sci. USA*, **1993**, *90*, 3745.

33 F. Zaccaria, G. Paragi, F. C. Guerra, *Phys. Chem. Chem. Phys.*, **2016**, *18*, 20895.

34 E. Largy, J.-L. Mergny, V. Gabelica, *Met. Ions Life Sci.*, **2016**, *16*, 203.

35 A. E. Engelhart, J. Plavec, Ö. Persil, N. V. Hud, in *RSC Biomolecular Sciences Nucleic Acid-Metal Ion Interactions*, ed. by N. V. Hud, **2008**, Chap. 4, pp. 114–149.

36 D. Varshney, J. Spiegel, K. Zyner, D. Tannahill, S. Balasubramanian, *Nat. Rev. Mol. Cell Biol.*, **2020**, *21*, 459.

37 T. G. Hoog, M. R. Pawlak, B. F. Bachan, A. E. Engelhart, *Biochem. Biophys. Rep.*, **2022**, 30, 101238.

38 F. Hao, Y. Ma, Y. Guan, *Molecules*, **2019**, 24, 1863.

39 I. Russo Krauss, A. Merlino, A. Randazzo, E. Novellino, L. Mazzarella, F. Sica, *Nucleic Acids Res.*, **2012**, *40*, 8119.

40 B. Pagano, L. Martino, A. Randazzo, C. Giancola, *Biophys. J.*, **2008**, *94*, 562.

41 A. Virgilio, D. Benigno, C. Aliberti, V. Vellecco, M. Bucci, V. Esposito, A. Galeone, *Int. J. Mol. Sci.*, **2023**, *24,* 15529.

42 D. Bhattacharyya, G. M. Arachchilage, S. Basu, *Front. Chem.*, **2016**, *4*, 38.

43 P. Serafini, M. Fernández-Leyes, J. Sánchez, R. B. Pereyra, E. P. Schulz, G. A. Durand, P. C. Schulz, H. A. Ritacco, *Colloids Surf. A Physicochem. Eng. Asp.*, **2018**, *559*, 127.

44 Unpublished data as follows. The mixture solution of the PBA having a thiol group at the 5′-position (5′-SH-PBA) and PPIX was prepared by the same protocol, and then a gold electrode was immersed into it for 24 h. After the repeated washing with the buffer solution, the electrode was immersed in the electrolyte, 1 M Na_2SO_4 solution, and electrochemical measurement was carried out by using a counter Pt electrode and Ag/AgCl reference electrode. Upon illumination of repetitive pulsed 650 nm light, the square waved photocurrent synchronized with the square waved light pulse was observed. The control electrode prepared in the absence of PPIX showed no photocurrent. In the presence of Triton®, PPIX molecules should be dispersed without aggregation and the PPIX was considered to prepare 1:1 complex with 5′-SH-PBA. Accordingly, the result indicates that a PPIX in the complex transferred electrons to the oxygen molecules saturated in the solution upon photoillumination. The complex was sufficiently stable because it was durable to repeated washing by buffer solution.

45 I. Russo Krauss, A. Merlino, A. Randazzo, E. Novellino, L. Mazzarella, F. Sica, *Nucleic Acids Res* **2012**, *40*, 8119.

46 I. Inamura and K. Uchida, *Bull. Chem. Soc. Jpn.*, **1991**, *64*, 2005.

47 J.-H. Fuhrhop, Demoulin Corinna, C. Boettcher, J. Konig, U. Siggel, *J. Am. Chem. Soc.*, **1992**, *114*, 4159.

48 B. Myrzakhmetov, P. Arnoux, S. Mordon, S. Acherar, I. Tsoy, C. Frochot, *Pharmaceuticals*, **2021**, *14*, 1.

49 S. M. Andrade, R. Teixeira, S. M. B. Costa, A. J. F. N. Sobral, *Biophys. Chem.*, **2008**, *133*, 1.

50 L. M. Scolaro, M. Castriciano, A. Romeo, S. Patanè, E. Cefalì, M. Allegrini, *J. Phys. Chem. B*, **2002**, *106*, 2453.

51 U. Siggel, U. Bindig, C. Endisch, T. Komatsu, E. Tsuchida, J. Voigt, J. -H. Fuhrhop, *Ber. Bunsennges. Phys. Chem.*, **1996**, *100*, 2070.

52 M. Kasha, H. R. Rawls, M. Ashraf El-Bayoumi, *Pure Appl. Chem.*, **1965**, *11*, 371.

53 A. Satake, Y. Kobuke, *Org Biomol Chem* **2007**, *5*, 1679.

54 C. A. Hunter, J. K. M. Sanders, *J. Am. Chem. Soc.*, **1990**, *112*, 5525.

55 K. Kano, K. Fukuda, H. Wakami, R. Nishiyabu, R. F. Pasternack, *J. Am. Chem. Soc.*, **2000**, *122*, 7494.

56 S. Faure, C. Stern, R. Guilard, P. D. Harvey, *J Am Chem Soc* **2004**, *126*, 1253.